OPTIMIZATION OF ORGAN FREEZING PROTOCOLS WITH SPECIFIED ALLOWABLE THERMAL STRESS LEVELS

Brian H. Dennis and George S. Dulikravich
Multidisciplinary Analysis, Inverse Design, and Optimization (MAIDO) Program
Department of Mechanical and Aerospace Engineering, UTA Box 19018
The University of Texas at Arlington, Arlington, TX 76019-0018, U.S.A.
Phone: +1 (817) 272-7376   FAX: +1 (817) 272-5010   E-mail: gsd@mae.uta.edu

Yoed Rabin
Biothermal Technology Laboratory, Department of Mechanical Engineering
Technion - Israel Institute of Technology, Haifa 32000, Israel
Phone: +972 4 829 2087   Fax: +972 4 832 4533   E-mail: yoed@tx.technion.ac.il

All correspondence should be sent to: George S. Dulikravich

ABSTRACT
A fully automatic procedure for maximizing the minimal local freezing rate in an organ while maintaining the local thermal stresses below a specified level throughout the arbitrarily shaped and sized three-dimensional organ made of different materials has been developed. This was achieved by determining correct variation of unsteady temperature distribution on the walls of the three-dimensional freezing container. A time-accurate finite element computer program was used to predict unsteady heat conduction with phase change and thermal stresses within the realistically shaped organs. A micro-genetic algorithm was then used to achieve nonlinear constrained optimization of time-varying container wall temperature distribution so that the prescribed maximum allowable thermal stress levels are never exceeded throughout the organ.

INTRODUCTION

One of the serious difficulties encountered by surgeons involved with organ transplantation is caused by the shortage of available organs. Using current organ preservation protocols which have the organ packed in ice at 4 degrees Celsius with a solution called UW (for University of Wisconsin) that is a mix of electrolytes, organs have the following average shelf lives from harvest to implantation: heart 4-6 hrs, lungs 4-6 hrs, kidney 24-48 hrs, and liver 36-48 hrs. A possible solution would be to establish an organ bank that could store organs with different immunological properties in a frozen state for lengthy periods of time. When preserving living human organs (kidney, heart, lungs, spleen, liver, bone, etc.) for the purpose of performing transplant surgery, the organ could be cooled in a special cryo-protective agent (CPA) gelatin while perfused by a cooling CPA liquid to a prescribed subfreezing temperature and kept at this temperature until used. If the cooling rate is too high, strong residual thermal stresses will cause fractures in the frozen tissues. If the cooling rate is too slow, chemical decomposition in the tissue will make the organ useless [1]. Experiments have shown that although a whole

organ does not survive freezing, cells and parts of the organ survive [2]. Thus, there has been a common belief that there is an optimal cooling rate for each particular type of tissue of an organ in order to maximize the survivability of the living cells and reduce the problem of future rejection by the organ recipient's body. Most of the controlled rate cooling devices currently in use [3] employ either a liquid cooling bath with ethanol or liquid nitrogen as the heat-exchange medium or a cooling chamber with vaporized liquid nitrogen as the coolant.

Freezing protocols that use a single optimal cooling rate at every point on the outside surface of an organ [2,4] result in considerably different values of local cooling rates inside the organ [5]. This situation, coupled with the possibility of rapidly changing thermal properties such as specific heat and thermal conductivity [5] near the phase front, makes the numerical modeling more difficult than in the case of simple heat diffusion.

One method that offers a possible practical solution to freezing and thawing of organs is to immerse them in a gelatin thus assuring that the heat transfer from the outer surface of the organ will occur by pure conduction. Numerical analysis of organ freezing [6] predicts that thermal boundary conditions are not propagated uniformly into the interior, resulting in a non-uniform distribution of temperature histories and cooling rates throughout the spatial domain.

A plausible objective could be to find the proper time variation of surface thermal conditions of the freezing container so that the optimal local cooling rates are achieved at each instant of time at every point in the organ. This concept was demonstrated as numerically feasible [7-12]. However, it has been impossible to preserve large organs even when the local cooling rates are apparently identical to those proven successful for small samples from the organ [2] because of the fractures caused by the thermal stresses. Other significant damaging mechanisms are ice crystal formation, blood vessel deterioration, and the toxicity effect of the CPA [13-16].

Thus, the objective during the freezing or thawing should not be to enforce experimentally obtained local optimal cooling rates since they apply to small tissue samples rather than whole organs. One of the main objectives should be to limit the thermal stresses that cause the fractures in the organs [13,15]. This paper deals with this particular objective.

MATHEMATICAL MODEL

The Navier equations for linear unsteady deformations u,v,w in three-dimensional Cartesian x,y,z coordinates are (inertia terms are expected to be negligible during the freezing or thawing)

$$(\lambda + G)\left(\frac{\partial^2 u}{\partial x^2} + \frac{\partial^2 v}{\partial x \, \partial y} + \frac{\partial^2 w}{\partial x \, \partial z}\right) + G\nabla^2 u + X = 0 \tag{1}$$

$$(\lambda + G)\left(\frac{\partial^2 u}{\partial x \, \partial y} + \frac{\partial^2 v}{\partial y^2} + \frac{\partial^2 w}{\partial y \, \partial z}\right) + G\nabla^2 v + Y = 0 \tag{2}$$

$$\left(\lambda + G\right)\left(\frac{\partial^2 u}{\partial x\,\partial z} + \frac{\partial^2 v}{\partial y\,\partial z} + \frac{\partial^2 w}{\partial z^2}\right) + G\nabla^2 w + Z = 0 \tag{3}$$

Here,

$$\lambda = \frac{E\nu}{(1+\nu)(1-2\nu)}, \qquad G = \frac{E}{2(1+\nu)} \tag{4}$$

where E is the Young's modulus and ν is the Poisson's ratio. The body forces per unit volume due to stresses caused by thermal expansion/contraction over the temperature range ΔT are

$$X = -(3\lambda + 2G)\frac{\partial(\beta\Delta T)}{\partial x} \tag{5}$$

$$Y = -(3\lambda + 2G)\frac{\partial(\beta\Delta T)}{\partial y} \tag{6}$$

$$Z = -(3\lambda + 2G)\frac{\partial(\beta\Delta T)}{\partial z} \tag{7}$$

This linear thermoelasticity system also includes unsteady energy conservation equation with latent heat of liquid/solid phase change lumped together with specific heat, that is,

$$\frac{\partial(\rho C_{effective}T)}{\partial t} = \nabla \cdot (k\nabla T) \tag{8}$$

The effective specific heat is a combination of the actual specific heat and the temperature variation of the latent heat, L, which is incorporated in the volumetric enthalpy, H, so that

$$\rho C_{effective} = \frac{\partial H}{\partial T} = \left(\frac{\nabla H \cdot \nabla H}{\nabla T \cdot \nabla T}\right)^{1/2} \tag{9}$$

All physical properties in this model are allowed to vary as function of space and temperature [17]. The latent heat was applied only in the mushy region, that is, at the points where the local instantaneous predicted temperature was between liquidus and solidus values. In systems of impure chemical composition, such as tissue, the phase change process involving release of latent heat is distributed over a range of temperatures rather than occurring at a single specific temperature. The nonlinear latent heat release can be modeled [6] by the application of the lever rule to the phase diagram for a binary, aqueous solution with a given initial composition. During CPA solidification the pattern of latent heat release implemented in the model may exhibit a strong influence on the calculated thermal histories.

DISCRETIZATION AND OPTIMIZATION

Due to its simple shape and the relative availability of thermophysical data, we chose to demonstrate this optimized freezing protocol concept on an example of a dog kidney. The kidney inner region (cortex), kidney outer region (medulla), and the spherical container shapes were created by first generating three concentric cubes. Each of the six faces of each of the three cubes was discretized with a structured grid of quadrilateral cells. The three concentric cubes were then transformed into three concentric spheres by dividing x,y,z coordinates of every grid point on every original cube with the radial distance of the corresponding point on the most outer cube. The six faces of the most outer cube then became the six deformed quadrilateral patches making up the surface of the spherical freezing container. The kidney medulla and the imbedded cortex spherical shapes were then analytically transformed into concentric ellipsoids that were consequently analytically bent. The surface grids consisting of deformed quadrilaterals (Fig. 1) were then connected with quasi-radial lines thus creating a fully boundary conforming three-dimensional structured grid. Each deformed hexahedron type grid cell was then partitioned into 24 tetrahedron type grid cells.

The surface variation of temperature on the spherical container wall was approximated with biquadratic Lagrange polynomials using 9 control points for each of the large six deformed quadrilateral patches forming the container wall thus resulting in a total of 26 design variables. Then, the transient temperature distribution was computed at every point of the organ. From this, the actual local cooling rates and thermal stresses were determined at each point of the organ. A nonlinear constrained function maximization method based on a genetic algorithm [20] was used after certain time interval, Δt, to optimize the temperature at each of the control points on the spherical container surface. That is, the new temperature distribution on the container walls was determined so that it maximizes the average cooling rate in the organ for the given time interval while keeping the local thermal stresses in the organ below a user specified maximum allowable value. The algorithm is outlined in Figure 2. The objective function, also referred to as fitness, F, that was maximized every time interval, Δt, was

$$ F = -\left[\frac{\Delta T}{\Delta t} + P\left(\frac{\sigma_{max}}{\sigma_{yield}} \right)^2 \right] \qquad (10) $$

where $\Delta T = T_{final} - T_{initial}$ and $\Delta t = t_{final} - t_{initial}$ and P is a user specified penalty term. Notice that the cooling rate is a negative number.

PHYSICAL PROPERTIES OF THE ORGAN AND THE CRYOPROTECTIVE GELATIN

Although the actual kidney is composed of four distinctive tissues: cortex (the most outer layer), medulla (the congruent inner layer), pelvis (the central domain), and fat (the domain that connects the pelvis with a part of the concave portion of the kidney surface), in this proof of concept example we have chosen to model the kidney as composed of only medulla and cortex.

Table 1. Specific heat and latent heat for unfrozen dog kidney tissues and the gelatin [17]

	Specific heat per unit volume: $\rho C = k/\alpha$ [J m^{-3} C^{-1}]	Latent heat per unit volume: $\rho \Delta H$ [J m^{-3}]
Cortex	3.68 x 10^6	250 x 10^6
Medulla	3.88 x 10^6	240 x 10^6
Gelatin	2 x 10^6	100 x 10^6

Table 2. Thermal conductivity and diffusivity for unfrozen dog kidney tissues and gelatin [17]

	Coefficient of thermal conductivity: k [J s^{-1} m^{-1} C^{-1}]	Coefficient of thermal diffusivity: α [m^2 s^{-1}]
Cortex	0.4905	0.1333 x 10^{-6}
Medulla	0.5065	0.1305 x 10^{-6}
Gelatin	0.3	0.13 x 10^{-6}

Table 3. Physical properties for frozen dog kidney bulk tissue and the gelatin

Properties & symbols	Kidney tissue	Gelatin	Reference
heat capacity per unit volume (frozen): ρC_S [J m^{-3} K^{-1}]	1.8 x 10^6	1.5 x 10^6	16; assumed
Thermal conductivity (frozen): k_S [J s^{-1} m^{-1} K^{-1}]	2.0	4.0	16; assumed
Temperature (liquidus): T [C]	0.0	0.0	assumed
Temperature (solidus): T_S [C]	-2.0	-2.0	assumed
Thermal expansion coefficient(frozen): β [C^{-1}]	0.6 x 10^{-4}	0.1 x 10^{-4}	16; assumed
Young's modulus of elasticity (unfrozen): E [N m^{-2}]	10 x 10^7	1 x 10^6	assumed
Young's modulus of elasticity (frozen): E [N m^{-2}]	10 x 10^9	1 x 10^9	16; assumed
Poisson's ratio (unfrozen): ν	0.333	0.333	assumed
Poisson's ratio (frozen): ν	0.333	0.333	assumed
Max. stress (unfrozen): σ [N m^{-2}]	1 x 10^6	0.5 x 10^6	assumed
Max. stress (frozen): σ [N m^{-2}]	132.2 x 10^6	50 x 10^6	14; assumed
Yield stress (unfrozen): σ [N m^{-2}]	0.5 x 10^6	0.4 x 10^6	assumed
Yield stress (frozen): σ [N m^{-2}]	65 x 10^6	50 x 10^6	14; assumed

NUMERICAL RESULTS

The system of equations (1-3) and (9) was integrated numerically using a finite element method on a tetrahedral non-structured grid, ILU and preconditioned Krylov subspace methods, object-oriented programming in C++ [18]. The accuracy of the finite element code for heat conduction involving solidification was verified though comparison with a known analytic solution [19]. The solidification of a liquid rod, which has an analytic solution, was simulated using a 3-D mesh of a rod composed of 480 parabolic tetrahedral elements. Figure 3 shows the variation of temperature with time for a specific point on the rod for both analytic and numerical solutions. The temperature was taken over a given time interval at a specific internal point inside the mesh. The numerical solution, though quite accurate is not exactly the same as the analytic solution. In our FEM implementation of the phase change, the temperature interval during which phase changes must be larger than zero. For calculating the rod case, a temperature interval of $1^{o}C$ was used. However, the analytic solution corresponds to phase change of a pure substance for which this temperature interval is zero. This non-zero temperature interval in the FEM model is the most likely source of the slight discrepancy between the numerical and the analytic results. A very small temperature interval for the phase change can be used. However, in this case it was found that an unreasonably small time step was required to obtain solutions with an almost perfect agreement with the analytic solution.

The three-dimensional freezing protocol simulation and optimization algorithm was then applied to a geometry composed of three domains. The outer boundary was a spherical freezing container. Within the container was a kidney consisting of a medulla and the imbedded cortex (Fig. 1). The optimizer was applied after every $\Delta t = 5$ minutes. The penalty term in the objective function, P, was fixed at P = 100 when the maximum von Mises stress in the kidney domain, σ_{max}, was greater than the local yield stress, σ_{yield}. The penalty term was P = 0 for all other situations. The genetic algorithm (GA) used 4 bit strings to represent each of the 26 design variables (container surface node temperatures). Each of these variables was allowed to vary from $20^{o}C$ to $-30^{o}C$. A uniform crossover operator was used with a 50% chance of crossover. A fixed population size of 31 was used with a 2% chance of mutation. Each optimization cycle was run for 20 generations. Each optimization cycle was executed on our distributed memory parallel computer made of commodity computer components. Each analysis run, which was composed of simulation of three-dimensional heat conduction with a moving freezing front in this multi-domain region including thermal stress analysis, required 3.5 minutes on a single CPU. Parabolic elements were used for heat conduction and linear elements were used for the stress analysis. The heat conduction grid was composed of 8245 nodes and 5184 tetrahedral elements. The stress analysis grid was composed of 1315 nodes and 5184 tetrahedral elements. A time step of 15 seconds was used for each transient heat conduction analysis.

Figure 4 shows the variation of the maximum stress found in the kidney domain for each of the optimized temperature distributions over time. Figure 5 shows the variation of the average cooling rate in the domain for each of the optimized temperature distributions over time. Notice that the cooling rate needs to be significantly reduced in the advanced stages of freezing. Figure 6 shows the temperature distribution for each time interval along a line formed by the

intersection of two cutting planes. Notice that by 50 minutes, the kidney has been completely frozen. It can also be seen that at some locations on the container surface the optimizer found that temperatures should increase after some time intervals (Figs. 7-9). This is caused by the imposed constraint on the maximum allowable local thermal stresses. A typical convergence history for the GA (Fig. 10) applied to the optimization of container surface temperature distributions shows that the GA finds improvements in only twenty generations. Similar proof of concept with the same software is possible for the optimization of thawing protocols where thermal stress is affected by the residual stresses developed during freezing [16].

CONCLUSIONS

In this first of a kind proof of concept simulation it has been demonstrated that it is possible to control the damage caused by the thermal stresses during freezing of organs by periodically optimizing temperature distribution on the surface of the freezing container. Using more accurate thermophysical data, finer spatial and temporal discretization, more diverse tissue sub-domains, and more geometrically complicated geometries of organs and containers is a relatively straightforward future extension of this work. A more challenging extension of this work would be to add internal perfusion during the freezing.

ACKNOWLEDGEMENTS

LITERATURE

1.   Mazur, P. (1970). *Science*, Vol. 168, pp. 939-949.
2.   Jacobsen, I.A. and Pegg, D.E. (1984). *Cryobiology*, Vol. 21, pp. 377-384.
3.   Kelley, F.D., Phelan, R. M. and Levin, R.L. (1982). *Cryobiology*, Vol. 19, pp. 372-391.
4.   Fahy, G.M. (1981). *Cryobiology*, Vol. 18, pp. 550-570.
5.   Hayes, L.J., Diller, K.R., Lee, H.S. and Baxter, C.R. (1984). *Cryo-Letters*, Vol. 5, pp. 97-110.
6.   Hayes, L.J. and Diller, K.R. (1983). *ASME J. of Energy Resources Technology*, Vol. 105, pp. 431-435.
7.   Hayes, L.J., Dulikravich, G.S. and Chiang, T.L. (1987). In: *Proceedings of 2nd ASME-JSME Thermal Engineering Joint Conference*, Honolulu, Hawaii, March 22-27, 1987.
8.   Madison, J.V., Dulikravich, G.S. and Hayes, L.J. (1987). In: *Proceedings of International Conference on Inverse Design Concepts and Optimization in Engineering Sciences (ICIDES-II),* G.S. Dulikravich (Ed.), The Pennsylvania State University, University Park, PA, October 26-28, 1987.
9.   Dulikravich, G.S. (June 1988). *Applied Mechanics Rev.*, Vol. 41, No. 6, pp. 270-277.

10.   Dulikravich, G.S. and Hayes, L.J. (1988). In: *Proc. of the Symposium on Computational Methods in Bioengineering,* ASME BED-Vol.9, pp. 255-265, R.L. Spilker and B.R. Simon (Eds.), ASME Winter Annual Meeting, Chicago, IL, Nov. 27 - Dec. 2, 1988.

11.   Dulikravich, G.S., Madison, J.V. and Hayes, L.J. (1989). In: *Proc. of 1st Pan-American Congress of Applied Mechanics (PACAM-II),* pp. 420-423, C.R. Steele and L. Bevilacqua (Eds.), Rio de Janeiro, Brazil, January 3-6, 1989.

12.   Ambrose, C., Hayes, L.J. and Dulikravich, G.S. (1989). In: *Proc. of National Heat Transfer Conf.,* AIChE Symposium Series 269, Vol. 85, pp. 440-405, S.B. Yilmaz (Ed.), Philadelphia, PA, August 6-9, 1989.

13.   Rabin, Y., Steif, P.S., Taylor, M.J., Julian, T.B., and Wolmark, N. (1996). *Cryobiology*, 33, pp. 472-482.

14.   Rabin, Y., and Steif, P.S., (1996). *Cryobiology*, 33, pp. 276-290.

15.   Rabin, Y., and Steif, P.S., (1998). *ASME J. of Appl. Mechanics*, 65, pp.328-333.

16.   Rabin, Y., and Steif, P.S., (2000). *Int. J. of Solids and Structures*, 37, pp. 2363-2375.

17.   Valvano, J.W., Cochran, J.R. and Diller, K.R., (May 1985). *International Journal of Thermophysics*, Vol. 6, No. 3, pp. 301-310.

18.   Dennis, B.H. and Dulikravich, G.S. (1999). *ASME Journal of Heat Transfer*, Vol. 121, pp. 537-545.

19.   Carslaw, H.S., and Jaeger, J.C., (1959). *Conduction of Heat in Solids*, Clarendon Press, Oxford.

20.   Dennis, B.H., Dulikravich, G.S. and Han, Z.-X. (1999). ASME paper 99-GT-441.
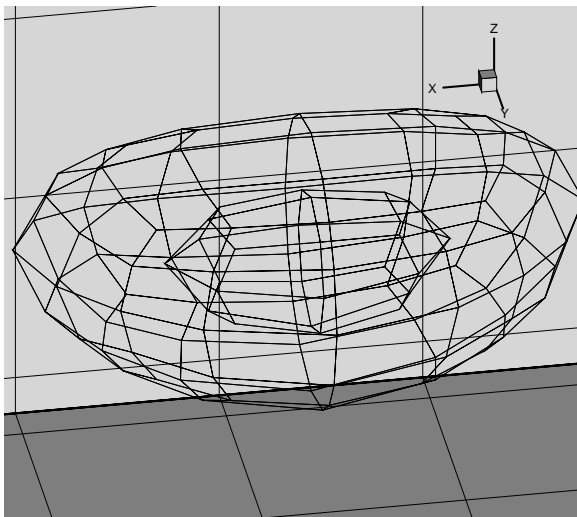
Figure 1. Surface grids for outer domain (medulla) and inner domain (cortex) of a kidney configuration.
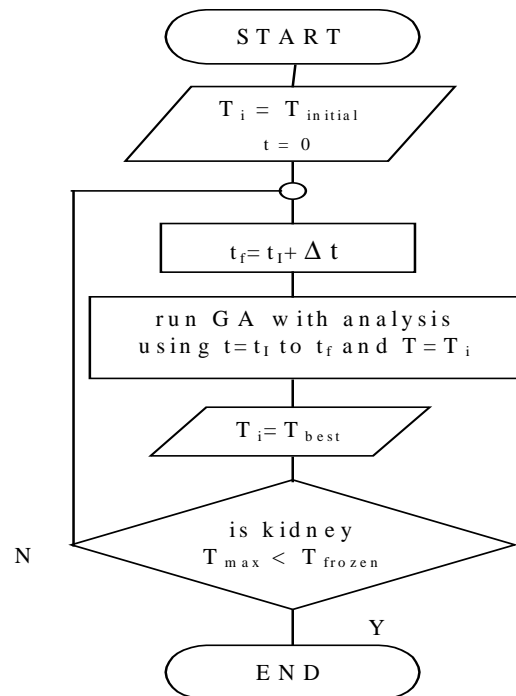

Figure 2. Algorithm for inverse determination of unsteady container surface thermal boundary conditions.
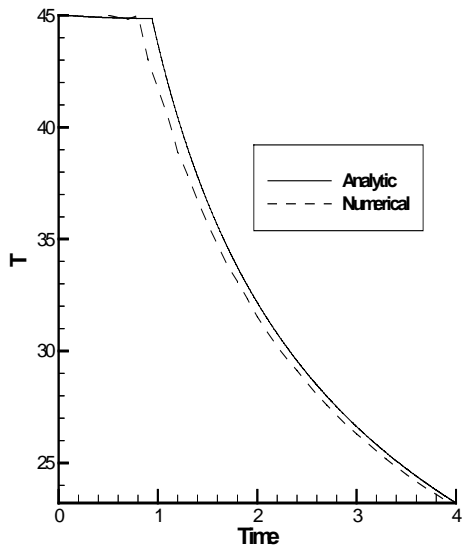
Figure 3. Comparison of analytic and numerical solutions for the freezing of a 1-D slab.
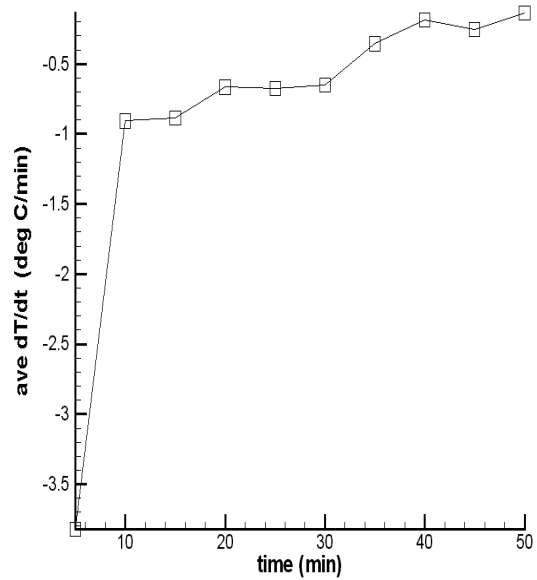

Figure 5. Time variation of average cooling rate in the kidney for optimized container surface temperature distributions.
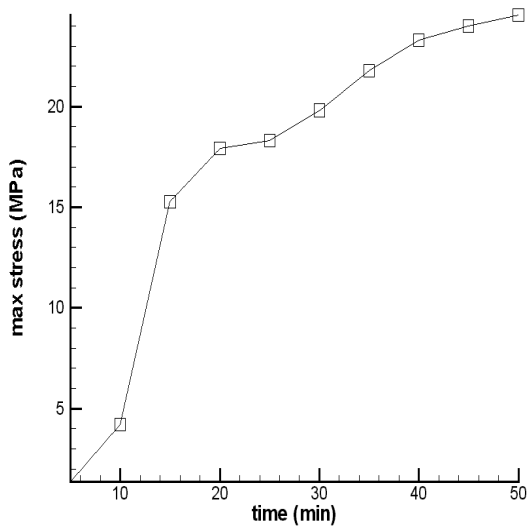

Figure 4. Variation of maximum stress with time for optimized container surface temperature distribution evolution.
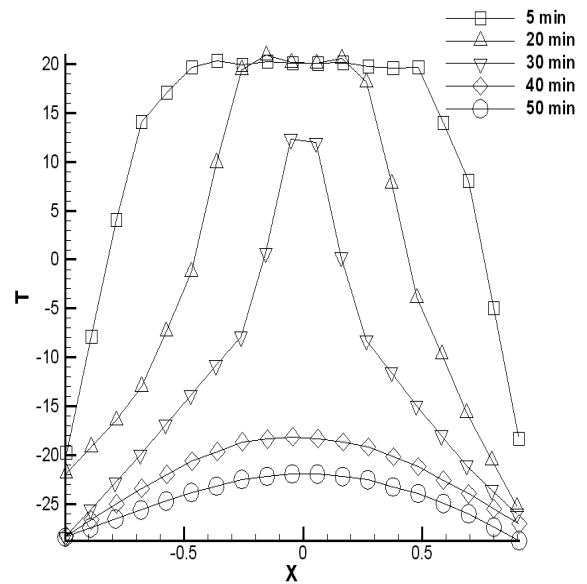

Figure 6. Temperature distribution in time along a line formed by the intersection of x-z plane and x-y plane (see Figure 1).
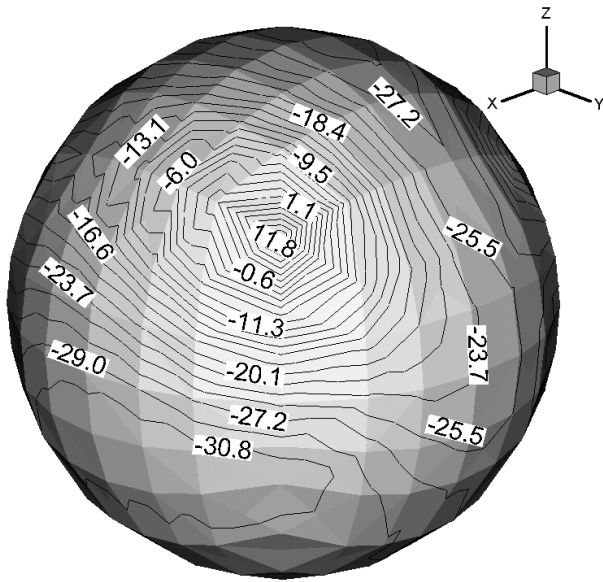
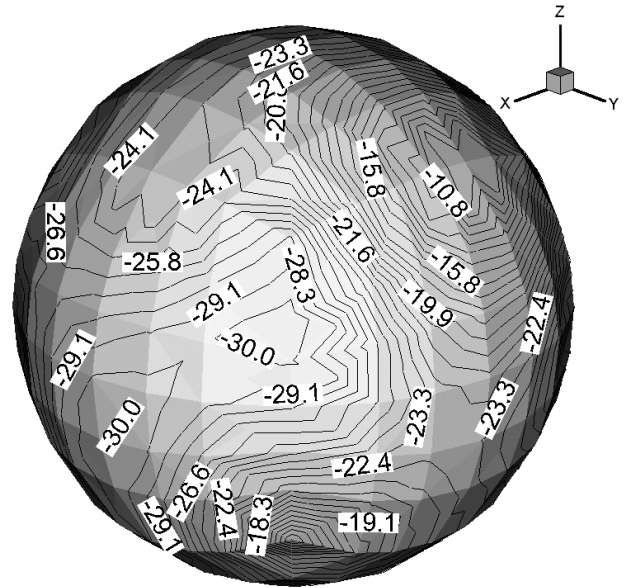Figure 7. Container surface optimized temperature distribution at 5 minutes.

Figure 9. Container surface optimized temperature distribution at 50 minutes.
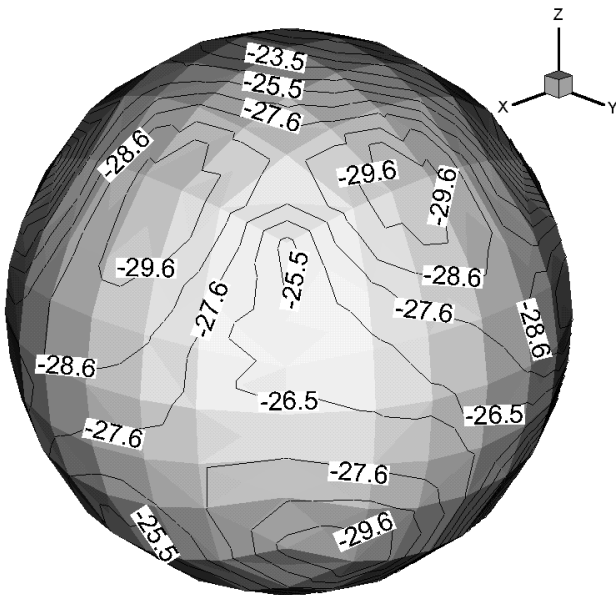

Figure 8. Container surface optimized temperature distribution at 30 minutes.
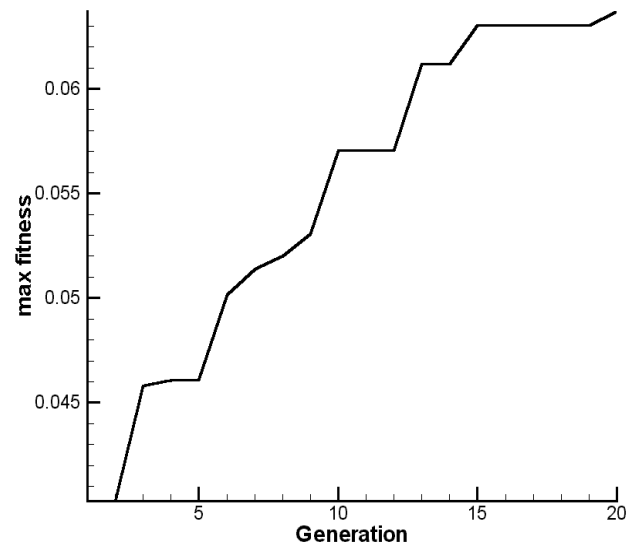

Figure 10. Typical convergence history for GA applied to the optimization of container surface temperature distribution evolution.